ECS Journal of Solid State Science and Technology, **5** (4) P3073-P3077 (2016)
2162-8769/2016/5(4)/P3073/5/$33.00 © The Electrochemical Society

JSS Focus Issue on Defect Characterization in Semiconductor Materials and Devices

Fermi-Level Effects on Extended Defect Evolution in Si^+ and P^+ Implanted $In_{0.53}Ga_{0.47}As$

A. G. Lind,[a,z] H. L. Aldridge, Jr.,[a] C. C. Bomberger,[b] C. Hatem,[c] J. M. O. Zide,[b] and K. S. Jones[a]

[a]*Department of Materials Science and Engineering, University of Florida, Gainesville, Florida 32611, USA*
[b]*Department of Materials Science and Engineering, University of Delaware, Newark, Delaware 19716, USA*
[c]*Applied Materials, Gloucester, Massachusetts 01930, USA*

The evolution of implant damage in InGaAs is studied for electrically active Si^+ and isoelectronic P^+ implants. Extrinsic loops formed by excess interstitials are shown to be less stable upon annealing for n-type Si^+ implants relative to isoelectronic P^+ implants. Damage created by P^+ implants into heavily n-doped InGaAs is also shown to be less stable than damage created by P^+ implants into unintentionally doped InGaAs indicating that the background doping concentration can significantly effect the evolution of implant damage upon annealing. Previous results have suggested that the electrical activation and diffusion behavior of n-type dopants, like Si in InGaAs, may be strongly influenced by vacancy concentration. TEM results in this study also suggest that heavy n-type doping in InGaAs results in the formation of a large population of vacancy defects that enhance the dissolution or inhibit formation of interstitial loops.
© 2015 The Electrochemical Society. [DOI: 10.1149/2.0141604jss] All rights reserved.

Manuscript submitted October 21, 2015; revised manuscript received December 4, 2015. Published December 17, 2015. *This paper is part of the JSS Focus Issue on Defect Characterization in Semiconductor Materials and Devices.*

Ion implantation is a useful means for introducing dopants into semiconductors but high implant doses often introduce a large number of point defects that form extended defects such as loops upon annealing. For future III-V fin-FET or nanowire devices, ion implantation may still play some role in dopant incorporation. In ion implantation it is desirable to avoid amorphization as the regrowth of amorphous material in fin-FET's result in highly defective regions.[1–3] To avoid amorphization, heated implants or implant doses below the amorphization threshold are used but large non-amorphizing doses often result in a large number of sub-threshold dislocation loop defects forming at or near the projected range. A more thorough classification of various type of implant damage in Si[4] and GaAs[5] is outlined in the works of Jones et al. but understanding of the evolution of extended defects in the non-amorphizing regime is of the most technological importance for $In_xGa_{1-x}As$. Previous works suggests that the Fermi level of group III-arsenides plays a significant role in modulating the type of point defects[6–8] and may influence the observed stability and population of extended defects formed by ion implantation in GaAs.[9,10] This work studies the effect of n-type doping on the stability of extended defects formed by ion implantation.

Experimental

Si^+ and P^+ implants were chosen as electrically active and isoelectronic implants to study the formation of extended defects from ion implantation in nominally un-doped and heavily n-doped $In_{0.53}Ga_{0.47}As$, referred to as InGaAs hereafter. Additionally, the nearly identical atomic mass and atomic radius of Si and P should result in nearly equivalent amounts of as-implanted damage and strain for the same implant dose and energy.

Si^+ or P^+ was implanted at 80°C with an energy of 20 keV and a dose of 6×10^{14} cm^{-2} into 300 nm of unintentionally doped InGaAs grown by metal-organic chemical vapor deposition (MOCVD) on semi-insulating InP. Van der Pauw Hall effect measurements of the as-grown MOCVD substrate indicated that the background doping of the substrate was nominally n-type with a background carrier concentration of 7.3×10^{16} cm^{-3}. Hall values in this report are based on raw data and are not corrected for the Hall scattering factor. The evolution of extended defects upon annealing at various temperatures and times from n-type, Si^+, and isoelectronic, P^+, implantation into the nominally un-doped substrate were then compared to determine what effect n-type doping had on defect evolution.

A heavily n-doped InGaAs film was also implanted with 20 keV, 6×10^{14} cm^{-2} P^+ at 80°C to determine the defect dissolution behavior of isoelectronic P^+ implants in heavily n-type films formed via epitaxial growth. The heavily doped InGaAs film was grown by solid source MBE at 490°C on a semi-insulating InP substrate. The InGaAs layer is 380 nm thick with the top 60 nm being heavily doped with Si resulting in a carrier concentration of 2.9×10^{19} cm^{-3}. Growth details of this film can be found elsewhere.[11] Damage evolution of the P^+ implants into the heavily doped MBE InGaAs film and nominally un-doped films were subsequently compared to determine what effect background doping had on extended defect dissolution.

After implantation and prior to annealing treatments, all films were encapsulated with a 15 nm thick Al_2O_3 film deposited by atomic layer deposition (ALD) to minimize surface degradation during annealing. Annealing treatments were performed with conventional rapid thermal annealing (RTA) with a ramp rate of 60°C/s to the dwell temperature ranging from 550–750°C and dwell times ranging from 5s to 900s. Post anneal characterization of extended defects was carried out using bright-field transmission electron microscopy (BF-TEM) and high-resolution transmission electron microscopy (HR-TEM). Cross-sectional TEM (XTEM) samples were made with a focused ion beam (FIB) using the h-bar technique and plan-view TEM (PTEM) specimens were made using a combination of mechanical pre-thinning and a modified h-bar technique which preserved the specimen surface. Post-implant Si and P profiles were obtained with secondary ion mass spectroscopy (SIMS) using 350 eV Cs^+ primary ion for sputtering.

Results

Si^+ and P^+ implants into nominally un-doped MOCVD InGaAs.— Fig. 1 shows the post implant Si^+ and P^+ concentration as a function of depth as determined by SIMS for a 20 keV, 6×10^{14} cm^{-2} implant at 80°C into the MOCVD $In_{0.53}Ga_{0.47}As$ substrate. Post-implant SIMS of the Si^+ and P^+ implants are shown to be co-incident at the peak of the implant profile and the projected range of these implants was determined to be 25 nm. It was observed from SIMS profiles that the MOCVD substrates have a large background P concentration from the MOCVD growth, roughly 1×10^{19} cm^{-3}. XTEM in Fig. 2 shows the effect that annealing temperature has on defect formation for isochronal 5s RTA treatments at temperatures from 550–750°C. Annealing treatments of 550°C for 5s for the P^+ implants, shown in Fig. 2a, exhibits some evidence of extended defect formation or implant damage. However, Si^+ implants more

[z]E-mail: aglind@ufl.edu

Downloaded on 2015-12-18 to IP 128.227.3.168 address. Redistribution subject to ECS terms of use (see ecsdl.org/site/terms_use) unless CC License in place (see abstract).

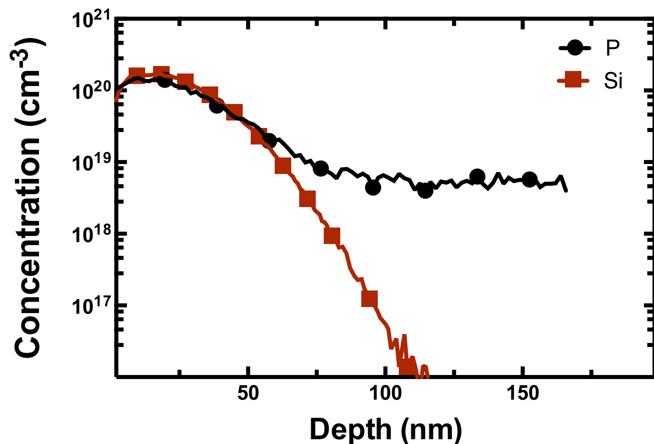

Figure 1. SIMS of as-implanted concentration profiles for 20 keV, 6 × 10^{14} cm^{-2} Si^+ and P^+ implanted at 80°C into MOCVD $In_{0.53}Ga_{0.47}As$.

clearly demonstrate evidence of defect formation upon annealing at 550°C, shown in Fig. 2b. This result is consistent with previous reports that activation of implanted Si requires annealing temperatures in excess of 550°C to promote damage recovery and cause Si activation in InGaAs.[12] Formation of extended defects is shown to increase with annealing at 650°C for 5s in the case of P^+ and Si^+ implanted in InGaAs, shown in Figs. 2c and 2d respectively. Comparison of the defects resulting from implantation of Si^+ and P^+ indicates that the defect density and morphology is very similar and a large density of <7 nm

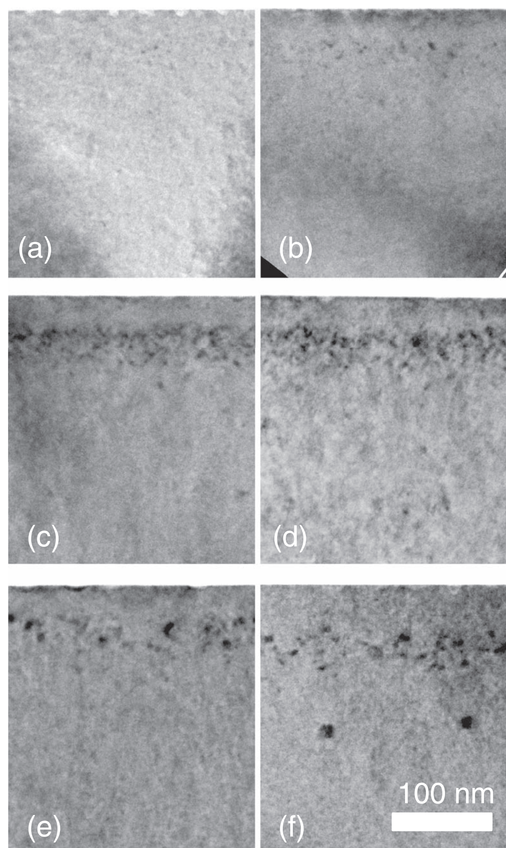

Figure 2. X-TEM of 80°C 20 keV, 6 × 10^{14} cm^{-2} (a) P^+ after 550°C 5s RTA, (b) Si^+ after 550°C 5s RTA, (c) P^+ after 650°C 5s RTA, (d) Si^+ after 650°C 5s RTA, (e) P^+ after 750°C 5s RTA, (f) Si^+ after 750°C 5s RTA.

sub-threshold loops are shown to form 25 nm below the surface, which is the projected range of the implants. For anneals of 750°C for 5s the density of defects from the P^+ and Si^+ implants, shown in Figs. 2e–2f, decreases relative to the 650°C anneal in Figs. 2c–2d. Extended defects occurring in the P^+ implanted material in Fig. 2e are shown to grow in size up to 15 nm and are still centered at the projected range. In the case of Si implanted material annealed at 750°C for 5s, shown in Fig. 2f, defects are shown to form beyond the 25 nm projected range while defects that nucleated closer to the surface have likely begun to dissolve. This observation is consistent with previous work that showed extended defects forming beyond the projected range.[13] It is evident from the micrographs presented in Fig. 2 that the nucleation of extended defects in Si^+ and P^+ implanted materials occurs at similar temperatures and at the onset of extended defect formation both species have similar densities. Direct comparison of defect density from XTEM assumes that sample lamellas are of constant thickness. However, the FIB lamellas in this study ranged from 80–110 nm thick. XTEM results in this study are shown primarily to indicate the depth at which defects are shown to occur which cannot be discerned from PTEM. Comparison of the defect location after annealing at 750°C indicates that Si^+ implants result in evolution of the defect band beyond the projected range as well as a reduction of loop defects in contrast to extended defects formed by P^+ implantation.

A second set of isothermal anneals were performed at 650°C for times ranging from 5s to 900s to observe the evolution of extended defects in Si^+ and P^+ implanted InGaAs using a combination of XTEM and PTEM. Figs. 3a–3d shows XTEM of P^+ implants after annealing at 650°C for times from 5–900s. P^+ implants are shown to exhibit ripening and increase in size from <5 nm to 15 nm loops. Figs. 3e–3h shows XTEM of Si^+ implants after the same annealing treatments. It is observed that the extended defects in the Si-implanted case do not exhibit significant ripening over the observed annealing times and the defect band caused by the implant is observed to become more diffuse with some defects observed well beyond the projected range. In the case of P^+ implants, the defect band remains at the projected range of the implant, consistent with the micrographs of isochronal annealing shown in Fig. 2. HR-TEM of a single loop defect resulting from the 20 keV, 6 × 10^{14} P^+ implant after annealing at 650°C for 320s from the sample shown in Fig. 3c is shown in Fig 4a. Fourier filtering of this defect, shown in Fig. 4b, was used to confirm the extrinsic nature of the defect loops. The extrinsic nature of the observed loops is confirmed by the extra planes of atoms consistent with other accounts of loop defects formed by ion implantation. Burger's circuit analysis of these images indicate that the loops are Frank partials with a Burger's vector of $a/3\langle 111\rangle$.

PTEM images for P^+ and Si^+ implants after annealing treatments at 650°C are shown in Figs. 5a–5h. It is also evident in plan view that extended defects occurring from P implantation and annealing for 10s, 40s, 320s and 900s in Figs. 5a–5d exhibit more ripening relative to Si implants after annealing for 10s, 40s, 320s and 900s in Figs. 5e–5h. With knowledge of the plan view defect density, average defect size and the planar atomic density of the $\{111\}$ plane ($d_{\{111\}} = 1.34 \times 10^{15}$ cm^{-2}), the number of interstitials bound to defect loops as a function of anneal time was estimated and is plotted in Fig. 6. The very small defects make it difficult to discern precisely the size of the dislocation core relative to the size of the defect observed from the strain contrast in TEM and as a result the actual population of interstitials bound to loops is likely overestimated from the micrographs. It is clear from the plot in Fig. 6 that the number of interstitials bound to loops after annealing at 650°C due to P^+ implantation is stable after 40s around 1.6 × 10^{14} cm^{-2} whereas longer annealing times for Si^+ implants result in a much lower number of interstitials, around 2.7 × 10^{13} cm^{-2}. The total number of interstitials bound in loops is shown to be less than the implanted dose of 6 × 10^{14} cm^{-2} for the implant conditions used in this work. Previous studies of lower dose As, Ge, and Se implants into GaAs have also shown no direct dependence on the interstitial population with implant dose and suggest that implant energy, or knock-on effects, and the electrical properties of dopants may also modulate population of interstitials.[5] In this study, energy

Downloaded on 2015-12-18 to IP 128.227.3.168 address. Redistribution subject to ECS terms of use (see ecsdl.org/site/terms_use) unless CC License in place (see abstract).

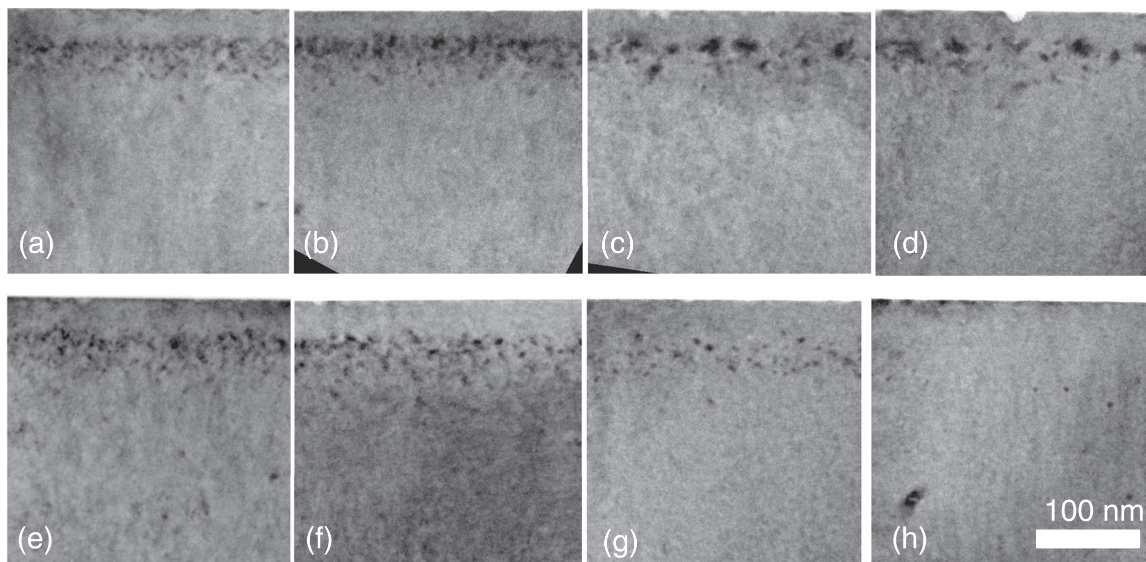

Figure 3. XTEM of 80°C 20 keV, 6×10^{14} cm^{-2} P^+ after 650°C RTA for (a) 5s, (b) 40s, (c), 320s, (d) 900s and 80°C 20 keV, 6×10^{14} cm^{-2} Si^+ after 650°C RTA for (e) 5s, (f) 40s, (g), 320s, (h) 900s.

and damage effects between the Si^+ and P^+ implants used are nearly identical suggesting that the observed differences in defect dissolution are related to electrical effects.

P^+ implants into unintentionally doped InGaAs and heavily n-type InGaAs.— 20 keV, 6×10^{14} cm^{-2} P^+ implants into the nominally un-doped MOCVD and the heavily doped MBE InGaAs films were annealed for 400s at 650°C to observe the defect evolution of isoelectric P^+ implants as a function of background n-type doping. SIMS of the MBE film, Fig. 7, shows that the peak of the P^+ implant is centered in the heavily Si-doped regions of the MBE grown layer. XTEM of the heavily doped MBE and unintentionally doped MOCVD films after 400s anneals is shown in Figs. 8a and 8b respectively. The micrographs in Fig. 8 indicate that small loops are still present in both substrates near the projected range of the implant. PTEM images of the same samples in Figs. 9a and 9b indicate that the unintentionally doped MOCVD films have 1.5×10^{14} cm^{-2} interstitials bound by loops while the heavily doped MBE films resulted in 1.5×10^{13} cm^{-2} interstitials bound by loops. The comparison of P^+ implants into both un-doped and heavily doped substrates suggests that the reduced nucleation of extended defects is not due exclusively to the implanted dopant species in InGaAs but also a result of the background electrical activation.

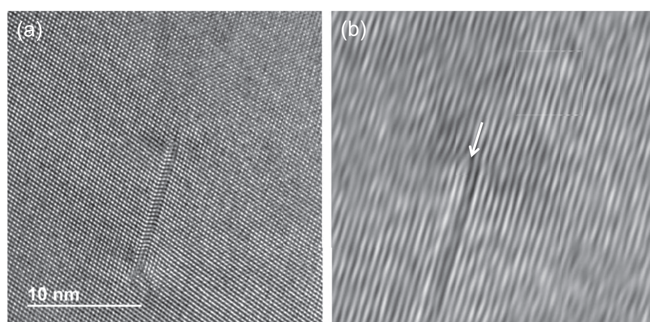

Figure 4. (a) HR-TEM of extrinsic loop formed by 80°C 20 keV, 6×10^{14} cm^{-2} P^+ implant after 320s 650°C RTA. (b) FFT highlighting extrinsic nature of defect loop.

Discussion

Previous work has observed dissolution of type II loop type defects formed by n-type Si^+ and Ge^+ implants into GaAs and InGaAs[10,14–17] while this work, more specifically, compares the defect evolution of n-type and isoelectronic implant species into InGaAs. The micrographs presented in this work indicate that extended defect evolution in InGaAs is very different for Si^+ and P^+ implants despite having nearly identical amounts of implant-induced damage for a fixed dose and energy. P^+ implant damage in InGaAs behaves in a manner that is consistent with most reports of non-amorphizing interstitial loops formed in other materials but Si^+ implant damage is shown to deviate from P^+ implant damage in a few ways.

XTEM of Si^+ implants shows that extended defect loops nucleates well beyond the projected range with increasing annealing times or temperatures whereas in the case of P^+ implants the defect band is shown to remain near the projected range with the same annealing treatments. Secondly, loop defects due to Si^+ implants do not show appreciable growth upon annealing and instead tend to dissolve and nucleate beyond the projected range whereas P^+ implants are shown to nucleate and grow with increasing annealing time, remaining centered about the projected range. Finally, P^+ implants into heavily n-doped and unintentionally doped InGaAs indicate that the evolution of extrinsic loops is dependent on the background electrical properties of the implanted material. These results suggest that the electrical properties of a given dopant species and the background doping of the InGaAs films play important roles in the evolution of extended defects in InGaAs. This effect is presumably due to large changes in point defect populations based on the Fermi level of the InGaAs.

In the case of heavily n-doped InGaAs and GaAs, the formation energy of group III vacancies (V_{III}) is calculated to rapidly decrease as the Fermi level is shifted near or into the conduction band resulting in a large increase in the population of vacancy defects formed by Frenkel pair formation.[6,18–22] Positron annihilation studies in GaAs have experimentally shown that heavily n-type regions result in vacancy rich regions but there is otherwise limited direct evidence of vacancies in n-type InGaAs and GaAs.[23–26] Previous studies have used the growth of interstitial loops formed by ion implantation as a means to detect increases in the interstitial defect fluxes in Si and SiGe[27,28] and in this work the reduced nucleation of interstitial loops in n-type material is seemingly evidence of an increase in the vacancy population in heavily n-type InGaAs.

Downloaded on 2015-12-18 to IP 128.227.3.168 address. Redistribution subject to ECS terms of use (see ecsdl.org/site/terms_use) unless CC License in place (see abstract).

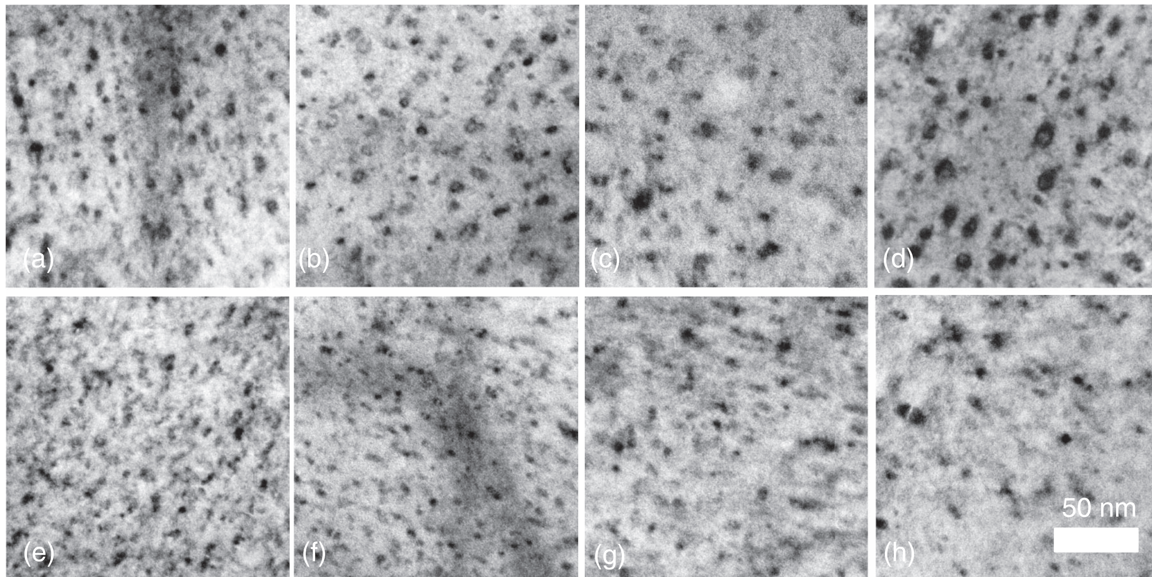

Figure 5. PTEM of 80°C 20 keV, 6 × 10^{14} cm^{-2} P^+ after 650°C RTA for (a) 10s, (b) 40s, (c), 320s, (d) 900s, and 80°C 20 keV, 6 × 10^{14} cm^{-2} Si^+ after 650°C RTA for (e) 10s, (f) 40s, (g) 320s, (h) 900s.

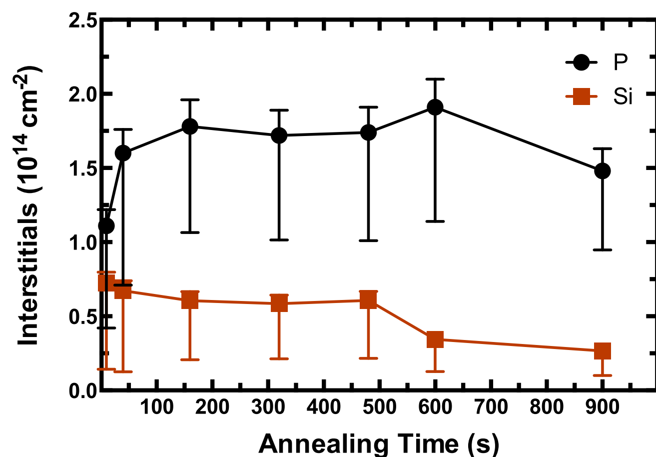

Figure 6. Areal density of interstitials bound to loops resulting from 80°C 20 keV, 6 × 10^{14} cm^{-2} Si^+ and P^+ implants as a function of annealing times ranging from 10–900s at 650°C.

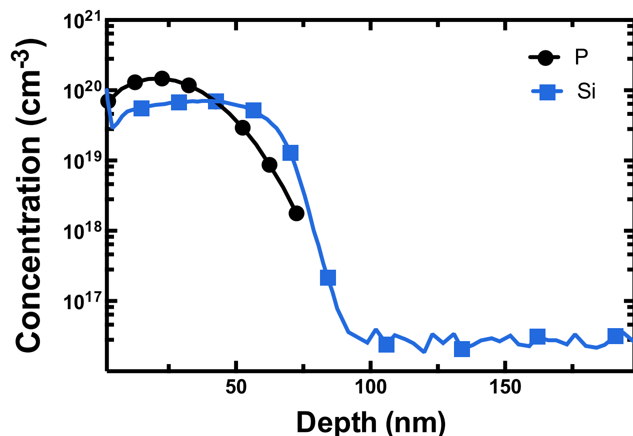

Figure 7. SIMS of as-implanted P^+ profile for a 80°C 20 keV, 6 × 10^{14} cm^{-2} into heavily Si-doped MBE $In_{0.53}Ga_{0.47}As$ substrate.

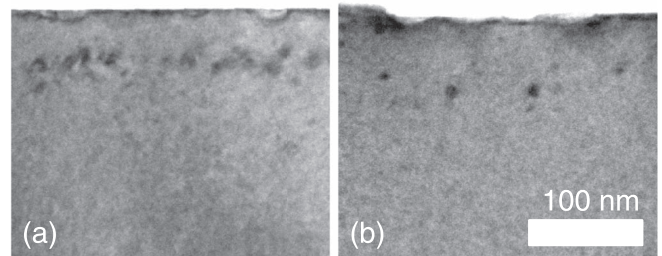

Figure 8. XTEM of 80°C 20 keV, 6 × 10^{14} cm^{-2} P^+ implant after 650°C RTA for 400s into (a) nominally un-doped MOCVD $In_{0.53}Ga_{0.47}As$ and (b) heavily Si-doped MBE $In_{0.53}Ga_{0.47}As$ substrate.

Previous experimenters have hypothesized that the large discrepancy between the electrically active and chemical concentration of ion implanted Si is due to amphoteric occupation of group III and group V sites by Si.[29] However, the formation of donor-vacancy complexes in InGaAs can also explain the observed electrical compensation of group IV and group VI, n-type dopants[30,31] as well as the concentration dependent diffusion present in heavily Si doped regions.[11,32,33] In the case of Si implants into nominally un-doped InGaAs, the high peak concentration of 1 × 10^{20} cm^{-3} of the implanted profile results

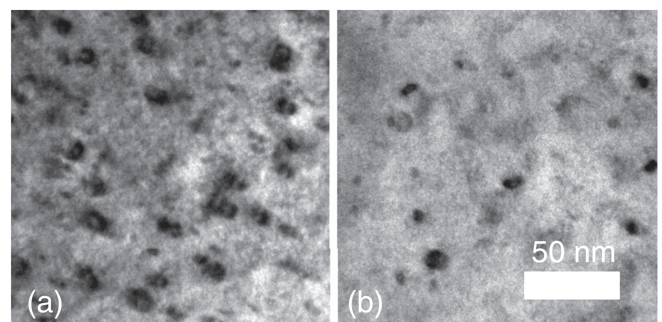

Figure 9. PTEM of 80°C 20 keV, 6 × 10^{14} cm^{-2} P^+ implant after 650°C RTA for 400s into (a) nominally un-doped MOCVD $In_{0.53}Ga_{0.47}As$ and (b) heavily Si-doped MBE $In_{0.53}Ga_{0.47}As$ substrate.

Downloaded on 2015-12-18 to IP 128.227.3.168 address. Redistribution subject to ECS terms of use (see ecsdl.org/site/terms_use) unless CC License in place (see abstract).

in a large amount of Si above the observed stable electrically active concentration of 1.5×10^{19} cm^{-3} that may be complexing with vacancies.[11] Vacancy complexing may result in a lower electrically active Si concentration relative to the chemical concentration of Si in the InGaAs film.

Shifts of the Fermi level toward the conduction band, occurring from high dose Si^+ implantation and activation, reduces the formation energy for V_{III} in III-V arsenides and can result in a large increase in vacancy defects.[18,24] V_{III} formed as a result of heavy n-type doping are free to consume the excess interstitials resulting from ion implantation. Isoelectronic P^+ implants will not move the Fermi level toward the conduction band and extended defects nucleate and grow without the influence of excess vacancies occurring due to Fermi level effects. Likewise, P^+ implants into the heavily doped n-type MBE InGaAs films show reduced nucleation relative to the same P^+ implant into unintentionally doped MOCVD InGaAs films. This effect is presumably due to a higher concentration of vacancies in the heavily doped substrate. Previous reports show also that the stability of isoelectronic Al^+ implant damage was improved by increasing the p-type background doping in GaAs[9] further suggesting that the Fermi level influences the stability of extended defects in III-V arsenides.

Previous experiments may also elucidate the observed dissolution and nucleation of defects in Si implanted InGaAs. Studies of heavily Si doped InGaAs sub-collectors in heterojunction bipolar transistors have indicated that the formation of group III Frenkel pairs ($V_{III} + i_{III}$) in the heavily doped subcollector act as a source of interstitials which enhance Zn diffusion in the base.[34] Interstitials resulting from Frenkel pair formation may be injected beyond the implanted Si concentration profile. This injection of interstitials into the bulk could then increase the interstitial saturation beyond the peak of the implant profile causing some defects to form beyond the projected range while defects nearer to the surface are able to dissolve during the anneal. There was no evidence from XTEM of loop defects forming beyond the projected range in the case of isoelectronic, P^+ implantation, presumably due to a lack of interstitial injection occurring from Frenkel pair formation.

Conclusions

In conclusion, sub-threshold defect loops from 20 keV, 6×10^{14} cm^{-2} Si^+ and P^+ implants are shown to exhibit similar concentrations and locations in InGaAs at the onset of nucleation upon annealing at 650°C for 5s. Evolution of extended defects formed from P^+ implantation in unintentionally doped InGaAs is observed to be more stable than extended defect formed by Si^+ implantation upon thermal annealing. The observed difference in implant damage evolution between P^+ and Si^+ implants is likely due to Si^+ doping shifting the Fermi level toward the conduction band which reduces the formation energy and thereby increasing the population of V_{III} defects. Similarly, decreased stability of extended defects formed by P^+ implantation in heavily n-type InGaAs relative to P^+ implants into nominally un-doped InGaAs further suggests that the defect evolution is highly dependent on Fermi level effects and not a species effect alone.

The presence of large vacancy populations in heavily n-doped InGaAs also agrees well with other experimental observations of implanted dopants such as the electrical compensation of Si and Se and the heavily concentration-dependent diffusion of Si.[32,35,36] This study also suggests that the formation of interstitial loops due to implantation may be an effective means of obtaining indirect evidence of vacancy populations in other materials systems that have highly Fermi-level dependent point defect populations.

Acknowledgments

The authors acknowledge the Major Analytical Instrumentation Center at UF for the use of their transmission electron microscopy and FIB facilities. Dr. Yong Yang at the university for Florida for the use of his multiprep and Intel who sponsored this work through a Semiconductor Research Corporation customization grant. C. C. Bomberger is supported by the NSF (DMR-1505574) and by the Delaware Space grant College and Fellowship Program (NASA Grant-NNX15AI19H). J. M. O. Zide is also supported by the NSF.

References

1. R. Duffy et al., *Appl. Phys. Lett.*, **90**, 241912 (2007).
2. R. Duffy et al., *Appl. Phys. Lett.*, **99**, 131910 (2011).
3. B. Wood et al., *VLSI Technology, Systems and Application (VLSI-TSA)*, 1, (2015).
4. K. S. Jones, S. Prussin, and E. R. Weber, *Appl. Phys. A*, **45**, 1 (1988).
5. K. S. Jones, in *Handbook of Compound Semiconductors*, Handbook of Compound Semiconductors. P. H. H. E. McGuire, Editor, p. 285, William Andrew Publishing, Park Ridge, NJ (1996).
6. W. Walukiewicz, *Phys. Rev. B*, **50**, 5221 (1994).
7. J.-L. Lee, L. Wei, S. Tanigawa, and M. Kawabe, *Appl. Phys. Lett.*, **58**, 1524 (1991).
8. J. Gebauer, R. KrauseRehberg, C. Domke, P. Ebert, and K. Urban, *Phys. Rev. Lett.*, **78**, 3334 (1997).
9. H. G. Robinson, K. S. Jones, M. D. Deal, and C. J. Hu, *MRS Proc*., **300**, 397 (1993).
10. K. S. Jones et al., *J. Appl. Phys.*, **70**, 6790 (1991).
11. A. G. Lind et al., *J. Vac. Sci. Technol. B*, **33**, 021206 (2015).
12. A. G. Lind, M. A. Gill, C. Hatem, and K. S. Jones, *Nuclear Inst. and Methods in Physics Research, B*, **337**, 7 (2014).
13. A. G. Lind et al., *Appl. Phys. Lett.*, **103**, 232102 (2013).
14. H. G. Robinson et al., *J. Appl. Phys.*, **76**, 4571 (1994)
15. E. L. Allen et al., *J. Electrochem. Soc.*, **138**, 3440 (1991).
16. A. G. Lind et al., *Ion Implantation Technology (IIT)*, 1 (2014).
17. C. P. Stewart, R. T. Blunt, G. R. Booker, and I. R. Sanders, *Physica B & C*, **116**, 635 (1983).
18. W. Walukiewicz, *Appl. Phys. Lett.*, **54**, 2094 (1989).
19. W. Walukiewicz, *Physica B: Condensed Matter*, **302**, 123 (2001).
20. S. B. Zhang, S.-H. Wei, and A. Zunger, *Physica B: Condensed Matter*, **273**, 976 (1999).
21. T. Y. Tan, H. M. You, and U. M. Gosele, *Appl. Phys. A*, **56**, 249 (1993).
22. F. El-Mellouhi and N. Mousseau, *J. Appl. Phys.*, **100**, 083521 (2006).
23. J.-L. Lee, L. Wei, S. Tanigawa, and M. Kawabe, *J. Appl. Phys.*, **68**, 5571 (1990).
24. J.-L. Lee, A. Uedono, S. Tanigawa, and J. Y. Lee, *J. Appl. Phys.*, **67**, 6153 (1990).
25. K. Wuyts, G. Langouche, M. Van Rossum, and R. E. Silverans, *Phys. Rev. B*, **45**, 6297 (2011).
26. J. Gebauer, R. Krause-Rehberg, C. Domke, P. Ebert, and K. Urban, *Phys. Rev. Lett.*, **78**, 3334 (1997).
27. J. K. Listebarger, K. S. Jones, and J. A. Slinkman, *J. Appl. Phys.*, **73**, 4815 (1993).
28. H. L. Meng, S. Prussin, M. E. Law, and K. S. Jones, *J. Appl. Phys.*, **73**, 955 (1993).
29. R. S. Bhattacharya, *Appl. Phys. Lett.*, **42**, 880 (1983).
30. D. T. J. Hurle, *J. Appl. Phys.*, **107**, 121301 (2010).
31. C. Domke, P. Ebert, M. Heinrich, and K. Urban, *Phys. Rev. B*, **54**, 10288 (1996).
32. H. L. Aldridge, A. G. Lind, M. E. Law, C. Hatem, and K. S. Jones, *Appl. Phys. Lett.*, **105**, 042113 (2014).
33. A. G. Lind, H. L. Aldridge Jr., K. S. Jones, and C. Hatem, *J. Vac. Sci. Technol. B*, **33**, 051217 (2015).
34. K. Kurishima, T. Kobayashi, and U. Gösele, *Appl. Phys. Lett.*, **60**, 2496 (1992).
35. A. Alian et al., *Microelectronic Engineering*, **88**, 155 (2011).
36. T. Penna, B. Tell, A. S. H. Liao, T. J. Bridges, and G. Burkhardt, *J. Appl. Phys.*, **57**, 351 (1985).

Downloaded on 2015-12-18 to IP **128.227.3.168** address. Redistribution subject to ECS terms of use (see **ecsdl.org/site/terms_use**) unless CC License in place (see abstract).